A Dynamic 3-D Surface Profilometer With Nanoscale Measurement Resolution and MHz Bandwidth for MEMS Characterization

Liang-Chia Chen, Yao-Ting Huang, and Kuang-Chao Fan

***Abstract*—Commercialization of microelectromechanical systems (MEMS) has made accurate dynamic characterization a major challenge in design and fabrication. In view of this need, a dynamic 3-D surface profilometer involving white light interferometric scanning principle with a stroboscopic LED light source was developed. The developed instrument was applied to a microcantilever beam used in atomic force microscopy (AFM) to analyze its full-field resonant vibratory behavior. The first five resonant vibration modes were fully characterized with vertical measurement accuracy of 3–5 nm and vertical measurement in the range of tens of micrometers. The experimental results were consistent with the outcomes of the theoretical simulation by ANSYS. Using stroboscopic illumination and white light vertical scanning techniques, the developed static and dynamic 3-D nanoscale surface profilometry of MEMS devices can achieve measurement range of tens of micrometers and dynamic bandwidth of up to 1-MHz resonance frequency.**

***Index Terms*—Dynamic profilometry, integrated mechatronics, microelectromechanical systems (MEMS) dynamic characterization, stroboscopic interferometry.**

I. Introduction

MICROELECTROMECHANICAL systems (MEMS), such as microaccelerometers, microbeams, micromembranes, and microbridges, possess component or system functionality essentially relying on the dynamic displacement properties of the microstructure and accurate characterization. In particular, this kind of characterization requires comprehensive knowledge of the vibration behavior of the MEMS. The design, performances, and reliability of MEMS and microoptoelectromechanical systems (MOEMS) depend critically on the control of the whole technology and especially on the knowledge and control of the mechanical behavior of materials and micromechanical devices [1], [2]. Characterization of the actual mechanical behavior of MEMS is essentially required since theoretical simulation cannot be performed due to possible dimensional imperfections, unexpected effects from inherent stress gradient, unpredictable real-boundary conditions, and damping mechanisms. Additionally, microstructure resonant frequencies can range from hertz to several megahertz, which significantly limits the range of measurement due to the increase in measurement bandwidth [3]. When performing stroboscopic interferometric measurement, the golden rule for freezing the moving interferometric fringe is that the larger the vibrating frequency is, the shorter the detecting strobed light should flash. When the vibrating period decreases to less than a few hundred nanoseconds, an excessively lengthy flashing time can lead to the degradation of interferograms caused by unwarranted image blurring.

In general, atomic force microscopy (AFM) possesses an atomically sharp probe tip affixed to a cantilevered beam, which is raster-scanned in close proximity over the surface of interest [4]. Most AFM cantilever beams are made of monocrystalline silicon. The resonance frequency and the force constant are mainly determined by the geometry and material properties of the cantilever beams. The thickness of the cantilever beam is generally measured using an interferometric microscope while the length and width are measured with an optical microscope. The resonance frequency and force constant can be estimated using the conventional flexural vibration equations. However, possible measurement errors and the assumption used in the calculation may cause 10%–20% errors when predicting the resonance frequency and force constant of cantilevers of 125–450 μm long [5]. Furthermore, for microdevices with internal residual stress, the vibration modes may significantly differ from that of unstressed microdevices [6]. Therefore, it is obvious that a single spectrum and point-type characterization are generally not sufficient for evaluating the dynamic behavior of either stressed elementary or complex AMF cantilever beams [4].

Heterodyne laser vibrometers, involving the laser Doppler effect and extensively used for MEMS vibration spectra measurements, have a typical detection limit below 10 pm in a frequency bandwidth of a few megahertz. They are insensitive to environmental noises and good for out-of-plane measurement [2]. However, such technique only obtains a point measurement of the out-of-plane vibrations and does not provide the essential information on the relative phase of the vibrations, thus, affecting the comprehensive understanding of dynamic behaviors of microdevices. To enhance the scanning efficiency, optical microscopic interferometry, digital holography (DH), and electronic speckle pattern interferometry (ESPI) can all be applied to full-field out-of-plane vibration measurements of M(O)EMS using either time averaging or stroboscopic techniques. Time-averaged interferometry with a fringe contrast function can

Manuscript received March 1, 2006; revised December 15, 2006. Recommended by Guest Editors H.-P. Huang and F.-T. Cheng. This work was supported by the Center for Measurement Standards (CMS) of the Industrial Technology Research Institute (ITRI), Taiwan, R.O.C., under a Cooperative Research Grant in 2005.

L.-C. Chen is with the Graduate Institute of Automation Technology, National Taipei University of Technology, Taipei 106, Taiwan, R.O.C. (e-mail: lcchen@ntut.edu.tw; s3618004@ntut.edu.tw).

K.-C. Fan is with the Department of Mechanical Engineering, National Taiwan University, Taipei 106, Taiwan, R.O.C., and also with Hefei University of Technology, Hefei 3345881, China (e-mail: fan@ccms.ntu.edu.tw).

Digital Object Identifier 10.1109/TMECH.2007.897268

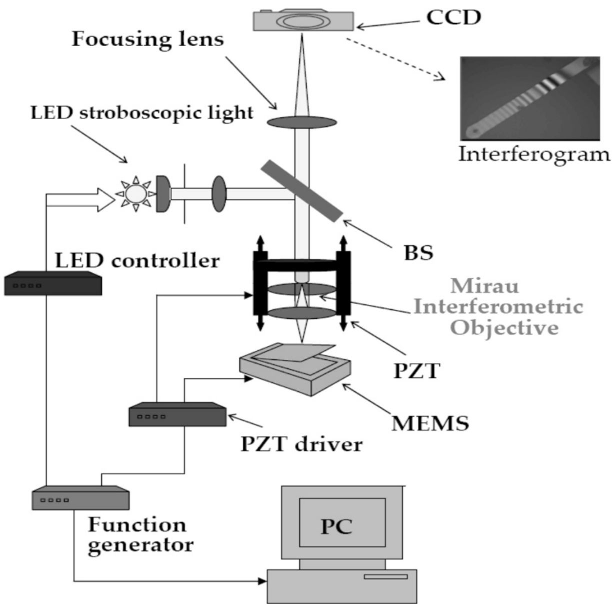

Fig. 1. Schematic diagram of the developed optical system.

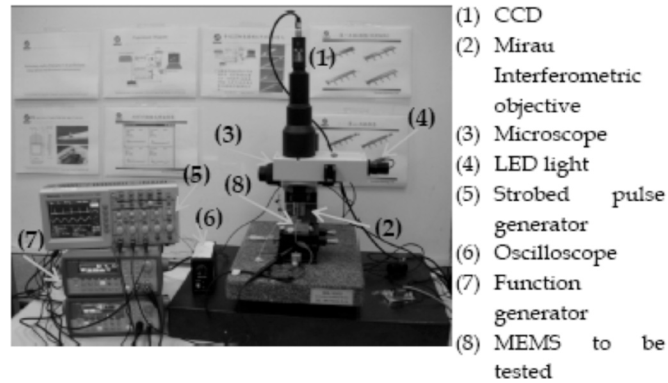

Fig. 2. Hardware setup of the developed optical system.

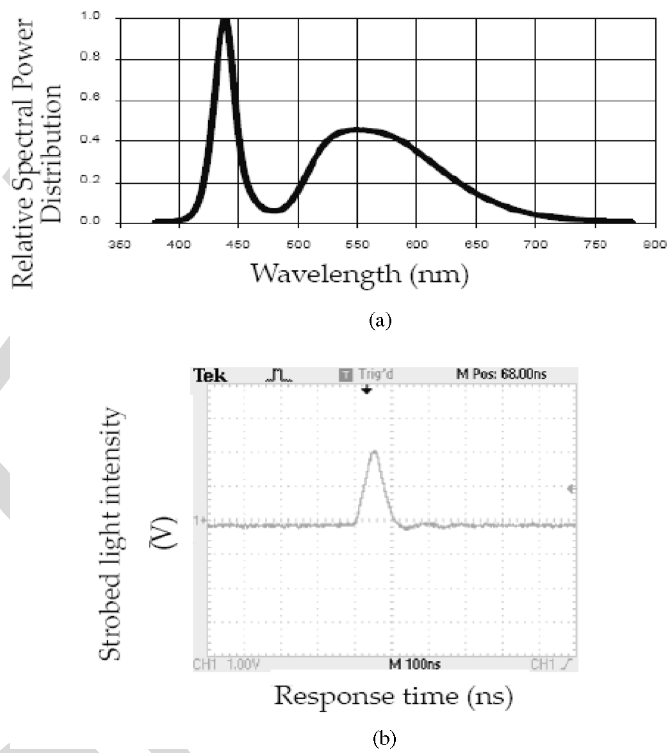

Fig. 3. Property of the LED light source. (a) Light spectrum. (b) Time response of the strobed LED light.

perform quantitative analysis of the interference pattern in contrast to obtaining vibration mode shapes, but is only suitable for low vibration frequency measurement. To overcome this problem, time-resolved stroboscopic measurements using either white light, single-wavelength LED light, or pulsed laser can be deployed for full-field interferometric techniques for 2-D or 3-D measurements of vibration mode shapes with a theoretical measurement bandwidth of up to 2 MHz [7]. The stroboscopic interferometry can be combined with phase-shifting algorithm as well as with fast Fourier transform (FFT) interferogram processing to obtain quasi-real-time 3-D profilometry of the vibration mode shape. Thus, this study develops a microscopic measurement system, involving white light stroboscopic interferometry and vertical scanning principle, to achieve full-field 3-D measurements in the range of tens of micrometers with nanoscale vertical resolution and high-bandwidth response of up to 1 MHz.

This paper comprises five sections organized as follows. Section II describes the system layout of the developed optical measurement system with its design of strobed LED light source and signal-synchronizing electronics. Stroboscopic vibration measurements analysis and interferogram processing are detailed in Section III. To demonstrate the feasibility of the proposed methodology, theoretical evaluation and dynamic vibratory measurements on AFM microcantilever beams with various operation modes were performed and analyzed in Section IV. Section V contains the conclusion and summarizes the development.

II. System Design and Integration

The optical system is established on a white light Mirau optical interferometer. As shown in Fig. 1, a standard Nikon microscope is equipped with Mirau interferometric objectives and a Physik Instrumente (PI) piezoelectric vertical translation system sensed by a capacitive positioning device for with the closed-loop control. The piezoelectric transducer with embedded capacitive sensors for closed-loop control has a 100-μm vertical translation range and a subnanometric resolution. The system was also equipped with a single LED (NSPW 300BS) having a maximum power output of 3 W. The LED can be driven in pulsed or continuous wave modes when incorporated with the light control circuit unit. The hardware setup of the developed optical system is shown in Fig. 2.

The light spectrum of the applied LED and the control circuit module are shown in Figs. 3(a) and 4, respectively. This arrangement enables a dual mode measurement capability in a single interferometer, where the continuous white light source can be applied for static surface profilometry while the stroboscopic

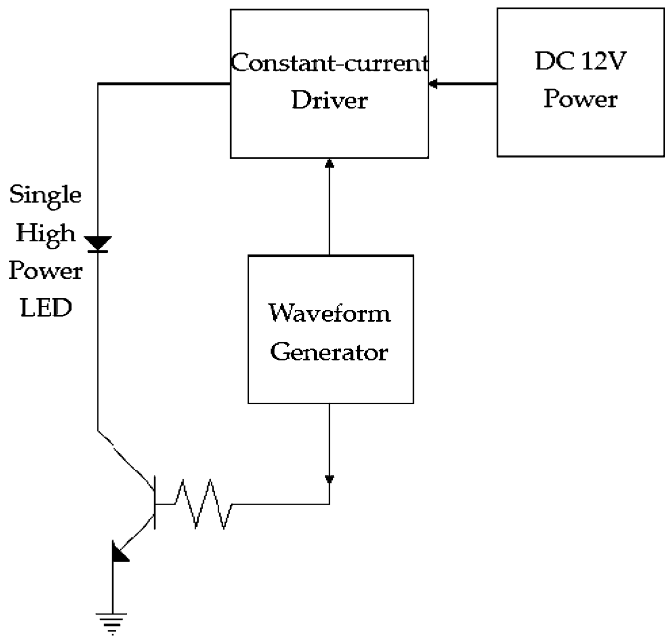

Fig. 4. Control circuit of the developed stroboscopic LED light module.

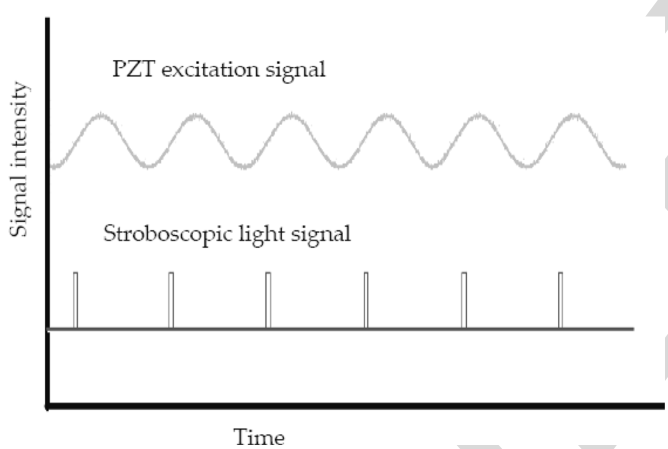

Fig. 5. Synchronized signals for stroboscopic signal and PZT vibration signal.

light source is utilized for dynamic vibratory measurements. The incident light from the light source module is collimated by a set of optical lenses for producing a parallel white light beam that illuminates the measured surface and reference mirror. A 5-V square signal with a duty cycle of less than 2% is employed to drive the control electronics of the stroboscopic LED. Meanwhile, the repeatability and timing accuracy of the LED firing electronics was evaluated by measuring the actual pulsed light with a photodetector (Thorlab PDA55 with a detection bandwidth of 10 MHz and sensible light spectrum ranging between 320 and 1100 nm). The time response of the light module can be seen in Fig. 3(b). The repeatability of the LED firing timing was identified to be within 2.1 ns for ± 1 standard deviation.

The MEMS testing sample is actuated by applying a sinusoidal voltage generated by a 20-MHz function waveform generator. The two driving signals mentioned earlier are accurately synchronized with an adjustable phase delay (shown in Fig. 5), in order to generate frozen interferograms. Although vibratory motion is damaging to the contrast quality of the conventional interferometric fringe images, this kind of stroboscopic source illumination is capable of capturing repeated images of the sample at the identical phase of oscillation such that the interference fringes can be unambiguously acquired. The whole system is mounted on a vibration-isolation optical table and placed in an environment with the minimum influence of external vibrations and disturbances. For the dynamic vibratory 3-D profilometry, the tested devices are rigidly secured on a silicon holder (*Pointprobe* silicon). The holder is mechanically fixed on a piezoelectric $\mathrm{Pb}_x\mathrm{ZrTiO}_{3(1-x)}$ (PZT) disk integrated with silver electrodes.

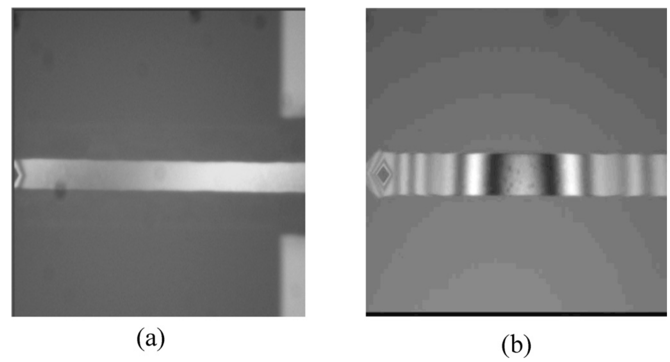

Fig. 6. AFM cantilever beam resonated at its secondary vibratory mode at a frequency of 1.067 MHz. (a) Blurred white light interferogram image when no strobed light was applied. (b) Good contrast interferogram image when a duty cycle of the strobed light set at 2% of the PZT driving signal was employed.

The measurement sensitivity and lateral resolution of the full-field out-of-plane vibratory motion of the developed system are primarily controlled by the diaphragm diameter and the global magnification of the optical system. With a 50-mm-diameter diaphragm and a $50\times$ Mirau objective, measurements of nanometric vibration amplitudes of MEMS with a spatial resolution equal to 1 μm and a frequency bandwidth of more than 2 MHz can be achieved. Compared with previous ones, the developed system has the following two technical advances in stroboscopic interferometric measurement.

1) *Single light source for both static and dynamic out-of-plane measurement*: A single superluminescent LED of white light spectrum can be operated either in pulsed- or continuous-wave modes when incorporated with the homemade light-control electronics. With the developed light module, the conventional white light interferometric measurement systems can be transformed into a system capable of dynamic characterization.

2) *Generation of shorter duty cycle of the strobed electric signal*: The contrast quality of frozen interferometric fringes is mainly determined by the period of the duty cycle and the response bandwidth of the driving light circuit. Experimental results have demonstrated that less than 2% duty cycle of the stroboscopic LED pulse can achieve dynamic response bandwidth of up to 2 MHz.

An AFM cantilever measured by the developed device is shown in Fig. 6, in which the cantilever is vibrated at its

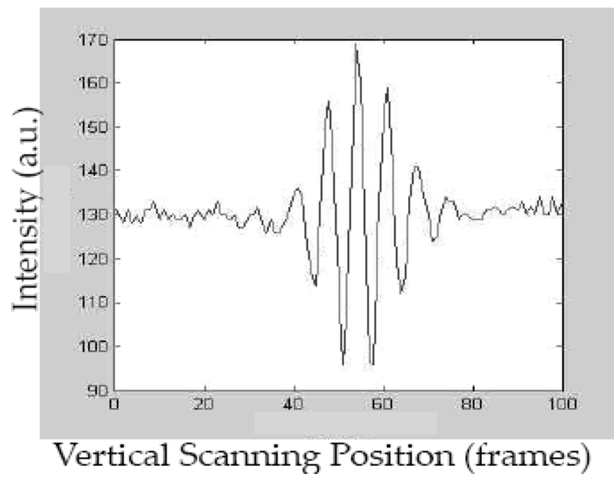

Fig. 7. White light scanning interferometric irradiance of static profile measurement of the Taylor Hobson standard step height.

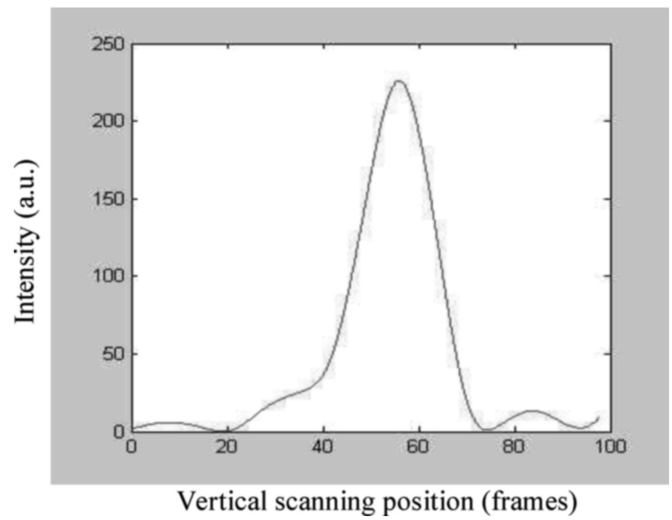

Fig. 8. Enveloped signal of the scanning interferometric irradiance shown in Fig. 7.

secondary vibratory mode with a frequency of up to 1.067 MHz. Fig. 6(a) displays its white light interferogram image when no strobed light was applied. In contrast, Fig. 6(b) shows the corresponding interferogram image when a duty cycle of the strobed light set at 2% of the PZT driving signal was employed to freeze the inteferometric fringes.

III. Stroboscopic Vibration Measurements Analysis and Interferogram Processing

In white light interferometry, the position of the zero-order interference fringe obtained from the white light interferometry (WLI) is independent of the wavelength of light [8]. When the maximum fringe contrast is identified, no height ambiguities and no focus errors exist in the measurement of surface microstructure. The detected intensity in the white light interferogram for the optical path difference $(2z)$ between two optical arms can be expressed as follows [5], [9]:

$$I(x, y) = I_o[1 + C(z)\cos(4\pi z/\lambda_{\mathrm{mc}} + \Delta\varphi)] \tag{1}$$

where

- I_0 background intensity;
- λ_{mc} apparent mean source wavelength;
- $\Delta\varphi$ local reflection phase shift difference;
- $C(z)$ global contrast function.

An example of white light scanning interferometric irradiance obtained by measuring the Taylor Hobson standard step height is shown in Fig. 7. A model of the interference fringe $I(x, y)$ can be further expressed by the following [9]:

$$\begin{aligned} g(z) &= \int_{k_l}^{k_u} \psi(k)\cos 2k(z - z_p)dk + C \\ &= m_c(z)\cos 2k_c z + m_s(z)\sin 2k_c z + C \end{aligned} \tag{2}$$

where

- k angular wavenumber $(k = 2\pi/\lambda)$;
- z_p height of the surface of the object at point (x, y);
- $\psi(k)$ energy distribution of the incident beam to the CCD detector with respect to k;
- k_c any fixed positive real number;

$$m_c(z) \text{ equals } \int_{k_l}^{k_u} \psi(k)\cos 2\{k(z - z_p) - k_c z\}dk;$$

$$m_s(z) \text{ equals } \int_{k_l}^{k_u} \psi(k)\sin 2\{k(z - z_p) - k_c z\}dk.$$

According to the definition of the interference fringe, the square envelope function is modeled as follows [9]:

$$\begin{aligned} r(z) &= \{m_c(z)\}^2 + \{m_s(z)\}^2 \\ &= \frac{2\Delta^2}{\pi^2}\left\{(1 - \cos\frac{\pi z}{\Delta})\{\sum_{n=-\infty}^{\infty}\frac{f(z_{2n})}{z - z_{2n}}\}^2\right. \\ &\qquad \left. + (1 + \cos\frac{\pi z}{\Delta})\{\sum_{n=-\infty}^{\infty}\frac{f(z_{2n+1})}{z - z_{2n+1}}\}^2\right\} \end{aligned} \tag{3}$$

where Δ is the sampling interval of the discrete interferometric fringes.

The square envelope function of the interference fringe obtained from WLI can be affected by some surface properties such as materials difference, surface roughness, and reflectivity. In addition, the inclined angle of the measured surface also affects the profile measurement since the reflected object beam cannot return back to the interferometer. Some of these challenges have been investigated in various cases [10], [11].

Using the aforementioned method, the static 3-D profile measurement can be reconstructed with the vertical resolution of up to 1 nm, and its repeatability within one standard deviation reaching a few nanometers. Figs. 8 and 9 illustrate the enveloped signal and the 3-D map reconstructed from the Taylor Hobson standard step height. The measurement accuracy has been demonstrated to be within 20 nm. The repeatability of static profilometry of the developed system was verified by measuring

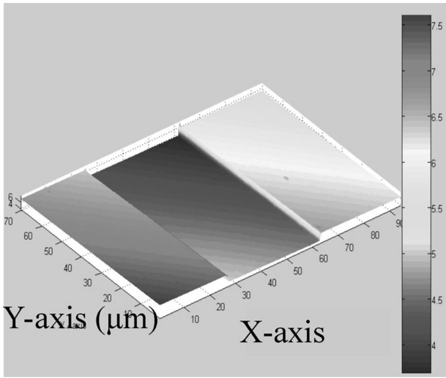

Fig. 9. 3-D profile measurement of the Taylor Hobson standard step height.

TABLE I
REPEATABILITY OF STATIC PROFILE MEASUREMENT USING THE DEVELOPED SYSTEM

Repeatability of Static Profile Measurement			
Test standard piece	Taylor Hobson, Step Height Standard (3700.0 nm)		
Measurement standard	ISO 5436-1 Geometrical Product Specifications (GPS)		
Number of measurements	30		
Magnification of Mirau Interferometric Objective	10X	20X	50X
Measurement variation within ±σ	20 nm	10 nm	4 nm

the step height $(3700.0 \pm 10.0\ \mathrm{nm})$ of the Taylor Hobson masterpiece for 30 times. The obtained data were evaluated using the International Standards Organization (ISO) 5436-1 Geometrical Product Specifications (GPS). Table I lists the measured results for three kinds of Mirau interferometric objectives.

The earlier equation is suitable for the case when the continuous LED light source is applied. When the stroboscopic LED light source is deployed, the contrast envelope has two peaks in its effective light power spectrum and the local vibration value $z(x/G, y/G)$ of the tested sample at the resonance frequency can be described as [2]

$$z(x/G, y/G) = z_0(x/G, y/G) + a(x/G, y/G)\sin(\omega t + \phi_1((x/G, y/G)) \quad (4)$$

where

- a vibration amplitude;
- f vibration frequency;
- ϕ_l phase lag between the driving signal and the device response;
- G interferometric objective magnification.

For stroboscopic measurements, the sample is illuminated during a light pulsed time δT short with respect to the vibration period $T = 1/f$. It can be demonstrated that if the duty cycle $\delta T/T$ is such that $\sin(n\delta T/T)/n\delta T/T) \cong 1$ for all harmonics present in the signal, the intensity detected in stroboscopic measurements is given by the following:

$$I(x,y) = NTI_0\left\{1 + C(z_0 + \Delta\phi + \alpha\sin(\omega t_0 + \phi_1)) \times \cos\left(\frac{4\pi}{\lambda_{mc}}z_0 + \Delta\phi + \frac{4\pi}{\lambda_{mc}}\alpha\sin(\omega t_0 + \phi_1)\right)\right\}. \quad (5)$$

Thus, when considering low vibration amplitudes and short light pulses such as $\sin(n\omega\delta T/2)/n\omega\delta T/2 \approx 1$, the detected intensity of stroboscopic inteferograms being accumulated N times is given as

$$I(x,y) = N\int_{t_0-\delta T/2}^{t_0+\delta T/2} I(x,y,t)dt \cong N\ \delta T\ I_0[1 + C(Z_0)\cos(B + \Delta\phi)]$$

$$\text{where}\quad B = \frac{4\pi}{\lambda_{mc}}z_0 + \frac{4_\pi}{\lambda_{mc}}\ a\sin(\omega t_0 + \phi_1) \quad (6)$$

TABLE II
DIMENSION SPECIFICATIONS OF THE TESTED AFM CANTILEVER BEAM

Technical Data	Typical Value	Typical Range	Specified Values
Thickness /µm	2	1.5 - 2.5	1.0 - 3.0
Mean Width /µm	50	45 - 55	42.5 - 57.5
Length /µm	450	445 - 455	440 - 460
Force Constant /(N/m)	0.2	0.07 - 0.4	0.02 - 0.77
Resonance Frequency /kHz	13	9 - 17	6 - 21

The aforementioned intensity is similar to the one for the static measurement when the interferometric image is frozen using stroboscopic light. Fig. 6(b) illustrates the interferogram of AFM probe cantilever beams measured by the developed device in which the image contrast is as good as the one for its static mode.

IV. EXPERIMENTAL DESIGN AND RESULT ANALYSIS

A. Description of AFM Cantilever Microbeams

For illustration, the static and dynamic surface profiles of a contact-mode AFM cantilever microbeam were measured by the developed device. The microcantilever was fabricated by NANOSENSORS Corporation, and its detailed material specifications can be found in TAble II.

Here, the material density (ρ), modulus of rigidity, Young's modulus, and yield strength of silicon were set at $2.33\ \mathrm{g/cm^3}, 0.5 \times 10^{11}\mathrm{N/m^2}, 1.69 \times 10^{11}\mathrm{N/m^2}$ (in the (1 1 0) direction), and $7 \times 10^9\mathrm{N/m^2}$, respectively. Meanwhile, the cross section of the underlying cantilever is trapezoidal, in which the beam has two geometrical widths—a smaller one on the tip side and a broader one on the opposite side. Thus, the mean width represents the median between these two values.

B. Mechanical Analysis of AFM Microcantilever Beams

An AFM cantilever beam, in general, can be illustrated as Fig. 10, in which the important dimensions of the beam and

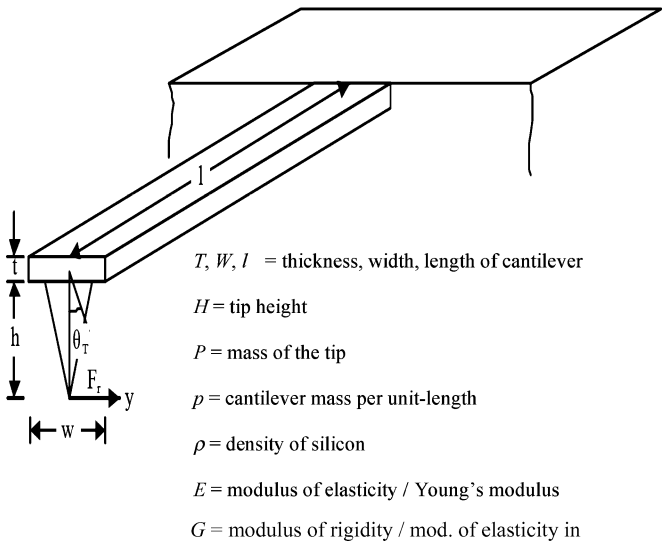

Fig. 10. Schematic diagram of an AFM cantilever beam.

probe tip are expressively depicted. By assuming that the beam is rigidly clamped at one end, the flexural resonant frequencies of a cantilever beam having a cross section A and an inertial moment I can be theoretically derived in (7) and [12]

$$f_n = \frac{\lambda_n^2}{2\pi}\frac{1}{L^2}\sqrt{\frac{E\mathrm{I}}{\rho\mathrm{A}}} \tag{7}$$

where

- n mode order;
- λ_n mode constant;
- A cross section of cantilever beam;
- L length of cantilever beam;
- E effective Young's modulus;
- I inertial moment;
- ρ density of the beam material.

Equation (7) does not take the probe tip into consideration. When taking the tip mass into account and assuming the tip as a cone with height h and base diameter equal to h, the corrected flexural resonant frequencies of a cantilever beam can be modeled as (8) [13]

$$f_{\mathrm{corr}} = \frac{\sqrt{3}}{2\pi}\sqrt{\frac{EWT^3}{12(PL^3 + 0.236pL^4)}} = 0.276\sqrt{\frac{EWT^3}{\rho(\pi h^3 L^3 + 0.283WTL^4)}}. \tag{8}$$

For most cases, the crystallographic orientation along the cantilever axis is aligned parallel to the (1 1 0) direction. According to the practical fracture limit used in the cantilever beam, the deflection of the cantilever at which the maximum stress in the lever equals 10% of the yield strength of the beam materials (1 1 0) can be expressed as

$$Y = \frac{1}{15}\frac{\sum \lim}{E}\frac{L^2}{T} \tag{9}$$

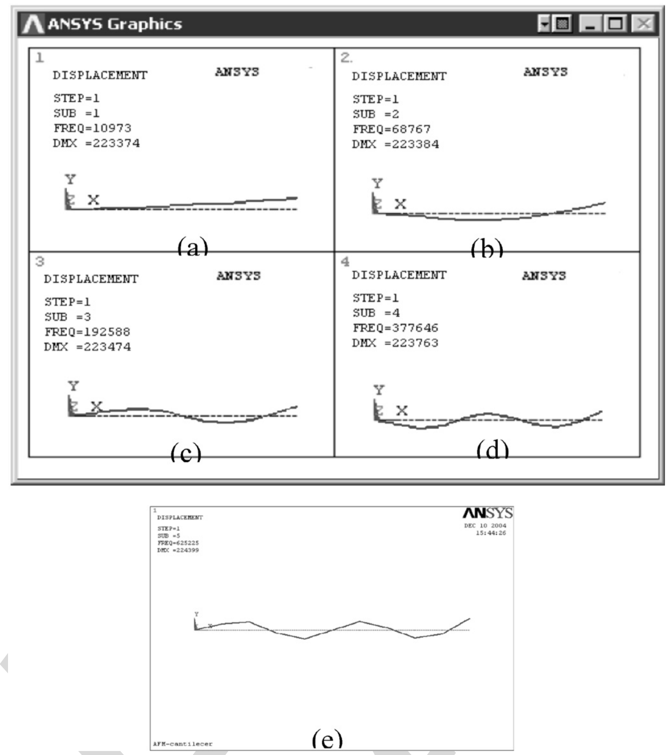

Fig. 11. ANSYS resonance analysis results of the cantilever obtained using ANSYS (the first five modes: (a), (b), (c), (d), and (e), respectively).

where Σ_{lim} is the yield strength of the beam material such as silicon.

C. Results and Analysis of the Theoretical Simulation

According to (8), a theoretical simulation on the beam dynamic analysis for identifying its vibration modes was performed using ANSYS. The first five modes were simulated and shown in Fig. 11, in which its predicted natural frequencies were 10.973, 68.767, 192.4, 377.5, and 623.9 kHz, respectively. To obtain the actual situation, the accurate mode frequencies were also measured by a laser Doppler interferometer and identified as 10.850, 68.60, 190.96, 387.0, and 643.2 kHz for the first five modes, respectively. It was noted that the predicted values were approximately consistent with the real values, and their differences increased slightly when the vibratory mode was increased from 1% to 5%. Such errors in simulation can be attributed to the deviations in dimensions and material properties of the cantilever.

D. Measurement Results and Analysis of the Dynamic Vibratory 3-D Shape of the AFM Microcantilever Beam

Fig. 12 shows the static 3-D surface profile obtained by the developed white light interferometric scanning method. As can be seen, the maximum deflection of the cantilever beam was less than 1 μm, which indicates that the beam was initially orientated at a relatively flat level. When performing the dynamic measurement of AFM cantilever beams, a 20-V_{pp} sinusoidal

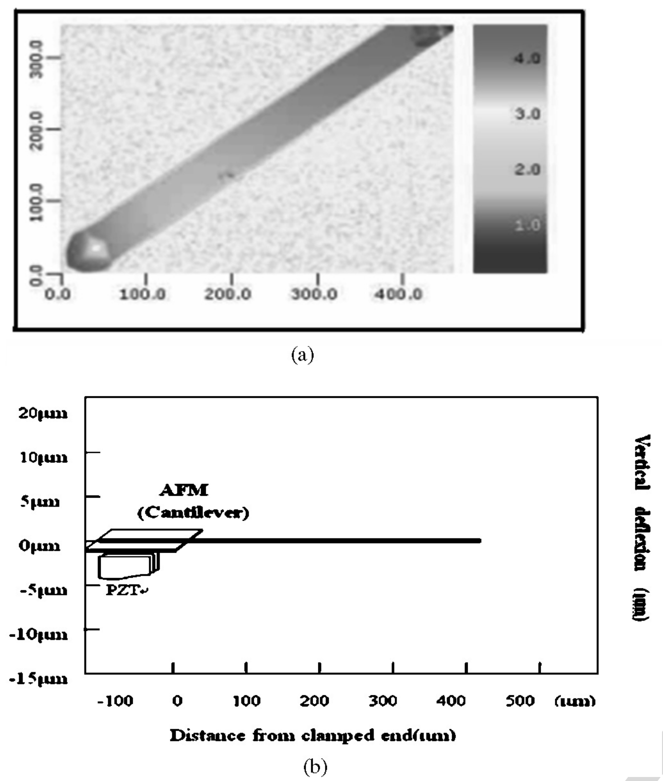

Fig. 12. Static 3-D measurement results of the AFM cantilever beam (contact mode). (a) Static 3-D profile. (b) Schematic diagram of beam deflection.

voltage with the five vibration mode frequencies was applied to the PZT driver, and a 2% duty cycle was used for the stroboscopic measurements. Stroboscopic measurements with white light vertical scanning interferometry of the vibration modes were performed at the first five frequency modes with a light pulse duty cycle of 2%. The LED and PZT driving signals were accurately synchronized with an adjustable phase delay.

Fig. 13 displays the first five resonance modes obtained using the stroboscopic measurement method developed. The measured mode shapes and cross section contours were obtained by profiling the vertical scanning contours along the microbeam length. The results were first corrected by the static deflection along the microbeam length. Theoretical mode shapes computed from the aforementioned ANSYS analysis were compared with the experimental ones and the two were convincingly consistent.

The slight inconsistency between the theoretical values and the measured ones may be attributed to the following two possible reasons.

1) *Dimension and material property deviation of the cantilever*: Potential measurement errors and the simplification used in the theoretical analysis may result in approximately 10% errors in the cantilever analysis.
2) *Inadequately clamped ends of the cantilever beam*: The cantilever beam is assumed to have ends perfectly clamped to its support base. Any inadequately clamped end may cause unexpected difference.

Dynamic measurement was also performed on a tapping-mode AFM cantilever beam (*Nanosensors NCLR*) with a different component specification. The second vibratory modes

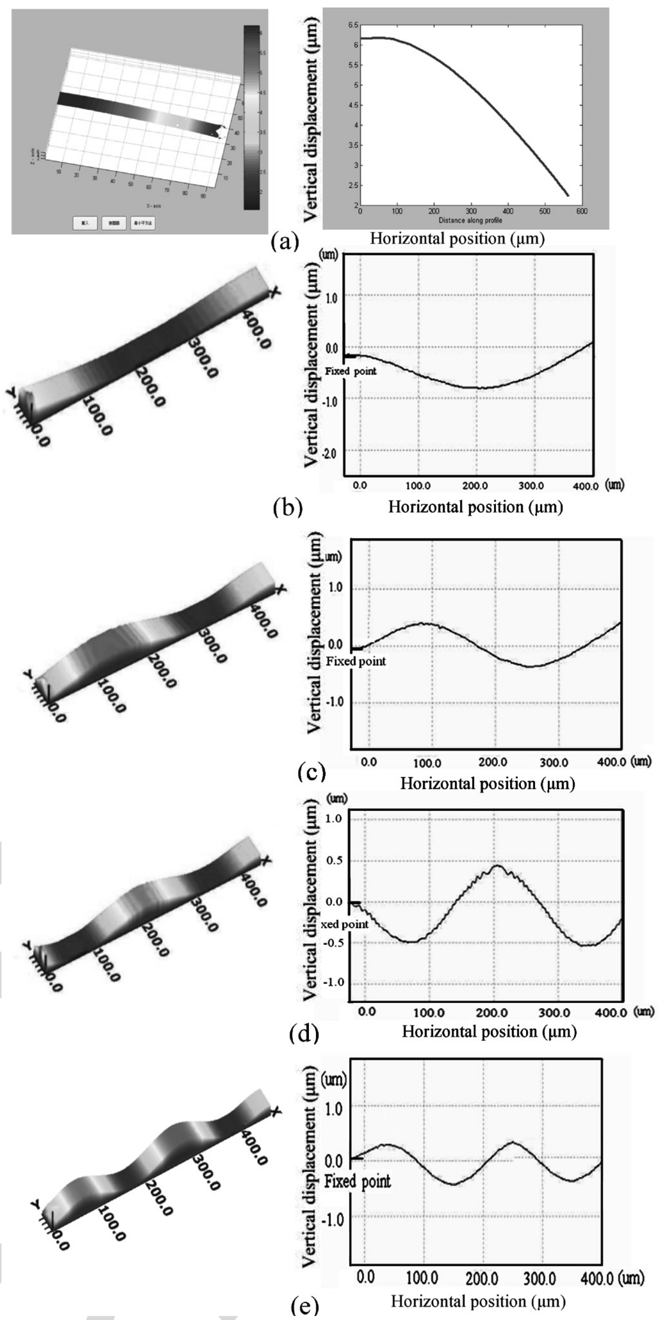

Fig. 13. 3-D map and cross section map of the first five resonance modes. (a)–(e) Sequentially represent the dynamic measurement results for the vibratory modes 1–5, respectively.

at 1192.1 kHz (the theoretical predicted value) was chosen to demonstrate the system capability in dynamic measurement at high resonant frequencies. By using a laser Doppler interferometer, the actual resonant frequency of this mode was identified as 1067 kHz. As shown in Fig. 14(a)–(h), the 3-D maps sequentially represent the dynamic measurement results for successively different cycle times while Fig. 14(i) displays the cross section of the vibratory shape having the maximum vibratory amplitude of 400 nm. The maximum vibration amplitude was within 400 nm. The results have clearly demonstrated the capability of the developed optical system and

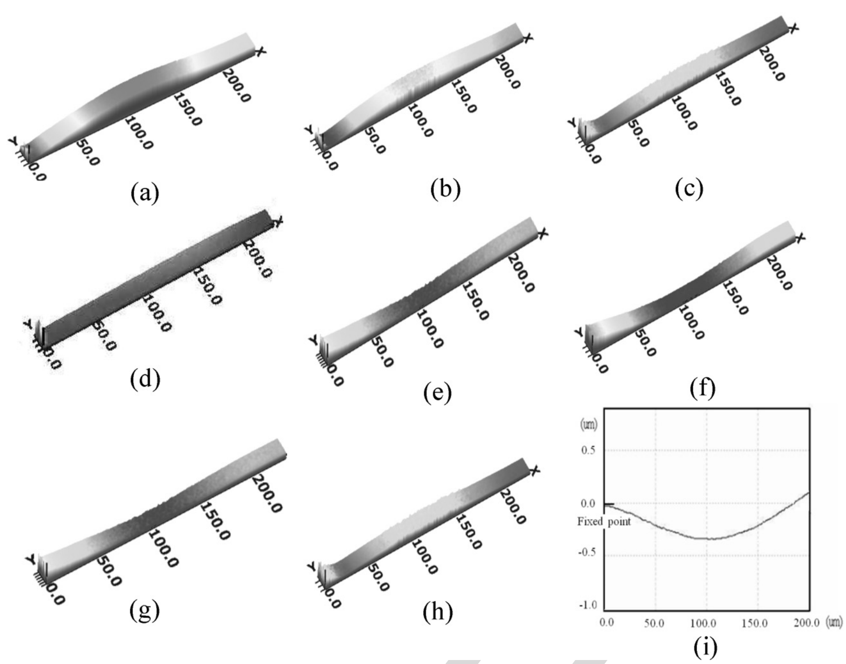

Fig. 14. Consequent 3-D vibratory maps of the second resonant mode (at frequency of 1.067 MHz). (a)–(h) Sequentially represent the dynamic measurement results for successively different cycle times, 12.5%, 25%, 37.5%, 50%, 62.5%, 75%, 87.5%, and 100%, respectively; and (i) displays the cross section of the vibratory shape having the maximum vibratory amplitude of 400 nm.

white light stroboscopic interferometry for the dynamic profile measurement of complex vibratory behaviors being operated at high frequency.

V. Conclusion

A dynamic surface profilometry involving white light interferometric scanning principle with a stroboscopic LED light source was successfully developed for dynamic characterization of AFM microcantilever beams. The experimental results demonstrate that the developed method is suitable for accurate full-field dynamic characterization of microdevices having complex vibratory behaviors, and a large depth of field (DOF) Q2 of hundredth micrometers can be achieved. The measured bandwidth of the vibration mode shape can reach up to 1 MHz with a depth detection resolution of 5 nm. Meanwhile, good agreement between the theoretical simulated outcomes and experimental results is found for 3-D vibratory characteristics of AFM microcantilever beams.

References

[1] S. M. Spearing, "Materials issues in microelectromechanical systems (MEMS)," *Acta. Mater.*, vol. 48, pp. 179–196, 2000.

[2] A. Bosseboeuf and S. Petitgrand, "Characterization of the static and dynamic behaviour of M(O)EMS by optical techniques: Status and trends," *J. Micromech. Microeng.*, vol. 13, pp. S23–S33, 2003.

[3] K. E. Speller, H. Goldberg, J. Gannona, and E. Lawrence, "Unique MEMS characterization solutions enabled by laser Doppler vibrometer measurements," *Proc. SPIE*, vol. 4827, pp. 478–485, 2002.

[4] S. Ryder, K. B. Lee, X. F. Meng, and L. Lin, "AFM characterization of out-of-plane high frequency microresonators," *Sens. Actuator A*, vol. 114, pp. 135–140, 2004.

[5] K.-C. Fan, L.-C. Chen, C.-D. Lin, C. C. Chang, C.-F. Kuo, and J.-T. Chou, "Development of dynamic 3-D surface profilometry using stroboscopic interferometric measurement and vertical scanning techniques," *J. Phys., Conf. Ser.*, vol. 13, pp. 51–54, 2005.

[6] S. Bouwstra and B. Geijelaers, "On the resonant frequencies of microbridges," in *Proc. Transducers*, 1991, vol. 1, pp. 538–542.

[7] M. R. Hart, R. A. Conant, K. Y. Lau, and R. S. Muller, "Stroboscopic interferometer system for dynamic MEMS characterization," *J. Microelectromech. Syst.*, vol. 9, no. 4, pp. 409–418, 2000.

[8] J. C. Wyant, "White light interferometry," Opt. Sci. Center, Univ. Arizona, Q3 Tucson, AZ.

[9] A. Hirabayashi, H. Ogawa, T. Mizutani, K. Nagai, and K. Kitagawa, "Fast surface profiling by white-light interferometry by use of a new algorithm based on sampling theory," *Appl. Opt.*, vol. 41, pp. 4876–4883, 2002.

[10] C. Quan *et al.*, "Study on the use of white light interferometry for multifiber-end surface profile measurement," *Opt. Eng.*, vol. 45, no. 5, p. 055603, 2006.

[11] C. Quan *et al.*, "Study on deformation of a microphone membrane using multi-wavelength interferometry," *Opt. Commun.*, vol. 197, pp. 279–287, 2001.

[12] R. D. Blevins, *Formulas for Natural Frequency and Mode Shape*. Melbourne, FL: Krieger, 1995, pp. 23–100.

[13] W. C. Young, *Roark's Formulas for Stress and Strain*. New York: McGraw-Hill, 1989, pp. 1–154.

Liang-Chia Chen was born in Taiwan, R.O.C., in 1963. He received the M.Sc.Eng. degree in mechanical engineering from National Taiwan University, Taipei, Taiwan, R.O.C., in 1989, and the Ph.D. degree in advanced manufacturing and mechanical engineering from the Centre for Manufacturing Research (CAMR), University of South Australia, Adelaide, Australia, in 2000.

Since August 2001, he has been an Associate Professor of automation technology at National Taipei University of Technology, Taipei. He was a Research Engineer with Gerard Industries of Australia for four years. His current research interests include automatic optical inspection (AOI), nanomaterials fabrication and control, reverse engineering for rapid manufacturing, and micro/nano 3-D surface profilometry. He has published two book chapters and more than 50 international conference papers. He has refereed 45 journal papers.

Dr. Chen is a Graduate Member of the Institution of Engineers of Australia and a member of the Society of Manufacturing Engineering.

Yao-Ting Huang received the M.S. degree in automation technology from National Taipei University of Technology, Taipei, Taiwan, R.O.C, in 2006.

His current research interests include image processing, automatic optical inspection (AOI), and nanometrology.

Kuang-Chao Fan was born in Taiwan, R.O.C., on January 4, 1950. He received the B.Sc. degree from National Taiwan University (NTU), Taipei, Taiwan, R.O.C., in 1972, the M.Sc. degree from the State University of New York at Buffalo, in 1976, and the Ph.D. degree from the University of Manchester Institute of Science and Technology, Manchester, U.K., in 1984, all in mechanical engineering.

He has been a Professor of mechanical engineering at NTU since August 1989. He was the Chairman of the Institute of Industrial Engineering, NTU, the Chairman of Chinese Institute of Automation Technology, the Director of the Tjing Ling Industrial Research Institute, and the Associate Dean of the Engineering College, NTU. Since 2001, he has been the Yangtze Professor at Hefei University of Technology, Hefei, China. His current research interests include manufacturing metrology, precision machining, machine tool technology, micro/nanomeasurement, optical switches, and tactile sensors.

Dr. Fan was the Chairman of the Society of Manufacturing Engineers (SME) Taipei Chapter.

QUERIES

Q1. Author: Please check the exapnsion of PI.
Q2. Author: Please explain "of hundredth micrometers" in Conclusion.
Q3. Author: Please provide the year for ref. [8].
Q4. Author: Please provide current affiliation of Y.-T. Huang.